Sample properties
at a cluster sensitivity of ~ 10^{-14} erg/s/cm2 in [0.5-2 keV]

F. Pacaud, and the XMM-LSS consortium

Abstract
We provide an empirical M(Fx,z) relation for clusters having z< 1.2
We investigate the relative role of sample size versus temperature accuracy in the determination of the evolution of the Lx-T relation.
We study the impact of the sample size, dispersion and amplitude in the scaling laws in the fitting of the cluster dn/dz .
For the complete cosmological modelling of the cluster number counts and correlation function: see contribution by Melin et al.

Working hypotheses
In all what follows, the clusters are assumed to belong to the Class 1, having a density of 6/deg^2 (see first contribution by Pacaud and PA07)
We performed an ab initio modelling of the observed number counts as follows: assume (1) a cosmological framework (ΛCDM) and a power spectrum along with a transfer function; (2) a mass function, (3) a halo model, (4) various scaling evolutionary relations for cluster physics. Then, for each redshift and mass range, the predicted luminosities are transformed into XMM count-rates using a dedicated plasma code. The C1 selection criteria are finally applied, resulting in a simulated observed redshift distribution

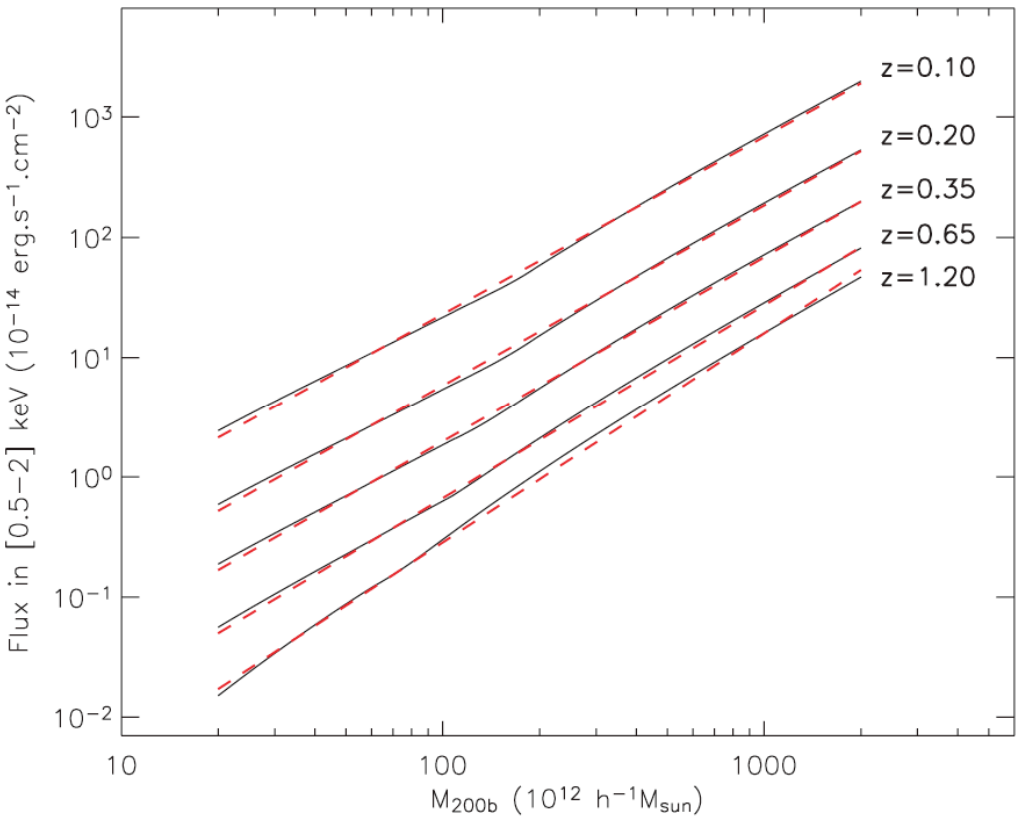

Figure 1. Mass-observable relations : is it usable?
Example: Calibration of the [0.5–2] keV band total flux versus M_200b relation.

Our model provides us with a tool for deriving heuristic mass-observable relations. For this purpose, we adopt the very general parameterisation introduced by Hu (2003):

$$OBS = OBS_O(M_d/M_O)^{p(z)}\, e^{A(z)}$$

The exact correlations derived from our model are shown for several redshifts with plain lines. The overplotted dashed lines show the recovered values from the fit, which is well reprensted by functionals of the form:

$$p(z) = p0 + p1\ z$$
$$A(z) = a0\ z^{a1}$$

The fits are better than 15 per cent over the $0.05 < z < 1.2$ and $2 \times 10^{13} < M < 2 \times 10^{15}$ h^{-1}Mo ranges. In practice, the intrinsic dispersion of the M–L relation also needs to be taken into account. Assuming $\sigma \ln L\ |M \sim 0.6$ (Section 5.1), this translates into a dispersion of –45 to +82 per cent in the flux–mass or count rate–mass relations. Thus, 'perfect' flux measurements may yield, via this formula, mass accuracies of the order of –60 to +100 per cent.
Such an empirical relation has obvious useful practical usages. It should be noted, however, that extrapolating the formulae in the present form above $z > 1.2$ is not straightforward as a number of prominent low-temperature lines (O VII, FeVII, FeVIII) are redshifted below the 0.5-keV boundary, creating discontinuities that cannot be accounted for with the above simple functionals.

Area	Temperature accuracy	σ_α	$N_{\mathrm{re-obs}}$
(deg^2)			
5	From the survey	0.59	–
20	" "	0.28	–
64	" "	0.15	–
5	10 per cent for the $z > 0.8$ clusters	0.58	2
20	" "	0.25	14
64	" "	0.14	41
5	10 per cent for the $z > 0.5$ clusters	0.50	9
20	" "	0.22	45
64	" "	0.13	139

Table 1: Expected accuracy in the determination of the evolution of the L_X–T (z) ∝ E(z)(1 + z)$^\alpha$ relation for various sizes of 10ks surveys, estimated from simulations.

It is assumed that the sample selection function is well determined (see contribution 1 by Pacaud), and that the uncertainty on cluster parameters mainly arise from statistical errors.
The temperature measurements are supposed to come either directly from the 10-ks XMM exposures, with the corresponding accuracy derived from the simulation results of Willis et al. (2005), or part of them to be improved by subsequent deep XMM observations, assuming an uncertainty of 10%; the last column gives the number of such clusters to undergo deep XMM pointings. σ_α is the mean 1σ error on α for a survey realization.

The simulations show that a significant improvement can be reached by increasing the sample size, provided that systematic errors can be kept below the level of statistical uncertainty: the accuracy on α scales roughly as the square root of the surveyed area. This is a very notable result, given that two-third of our clusters have no more than 500 counts available for the spectral fit. The spectral accuracy is of the order of 20 per cent below 2 keV, and 50 per cent around 5 keV (Willis et al. 2005), the latter concerning mostly distant clusters. The simulations further show that increasing the accuracy of the temperature measurements does not yield a very significant improvement in the evolution of the L_X–T relation – compared to the amount of time that would be necessary to obtain accurate temperatures for the $0.5 < z < 1$ hot clusters. This is mostly due to the fact that the dispersion in the L_X–T relation itself is large.

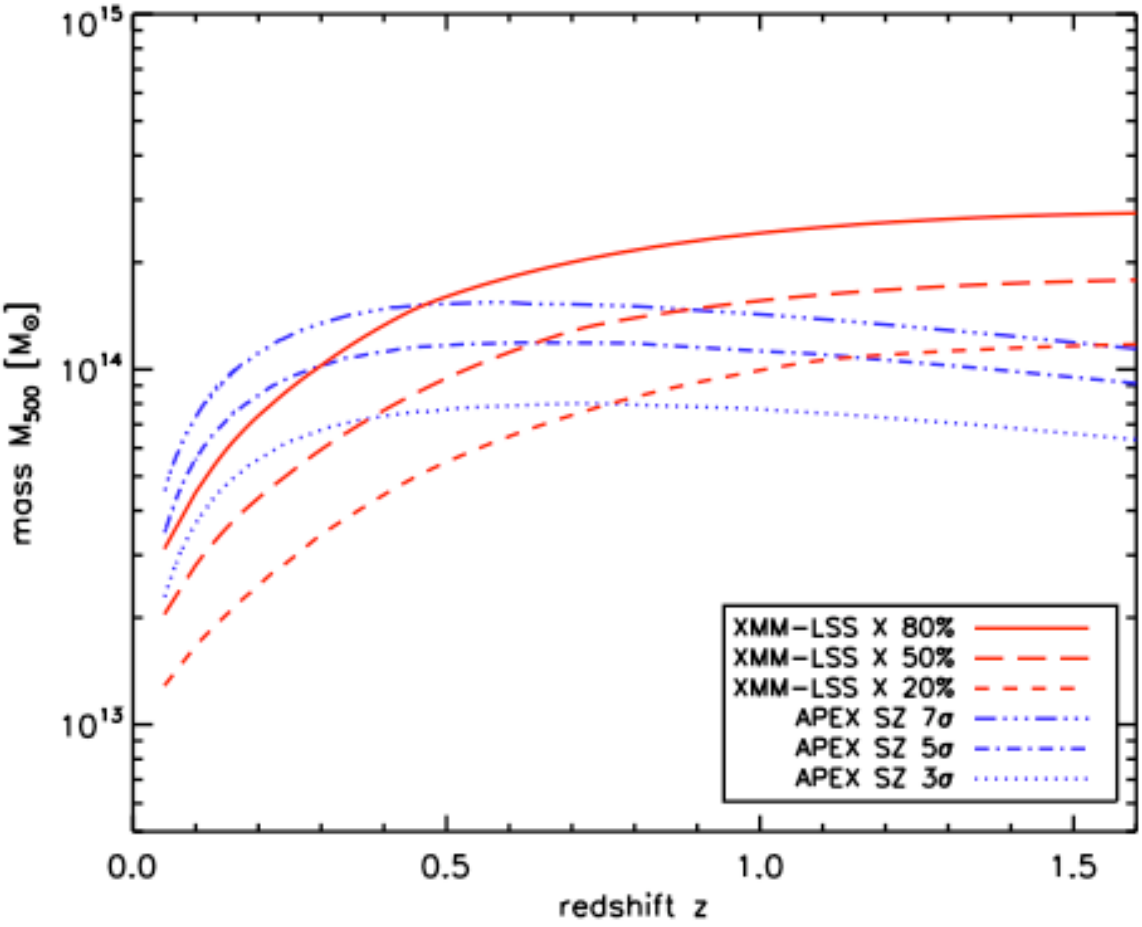

Fig. 2 Comparison between X-ray and Sunyaev-Zel'dovich sensitivities in terms of limiting cluster mass.
The red lines show various *measured* detection probability thresholds for C1 cluster population. The blue lines are the *predictions* for the APEX survey, currently observing the XMM-LSS field. These assume a noise r.m.s. of 10μK in two observing bands at 150 and 220GHz. For the regime of interest ($z < 1$), the X-ray observations are at least as efficient as the S-Z ones in terms of cluster detection.

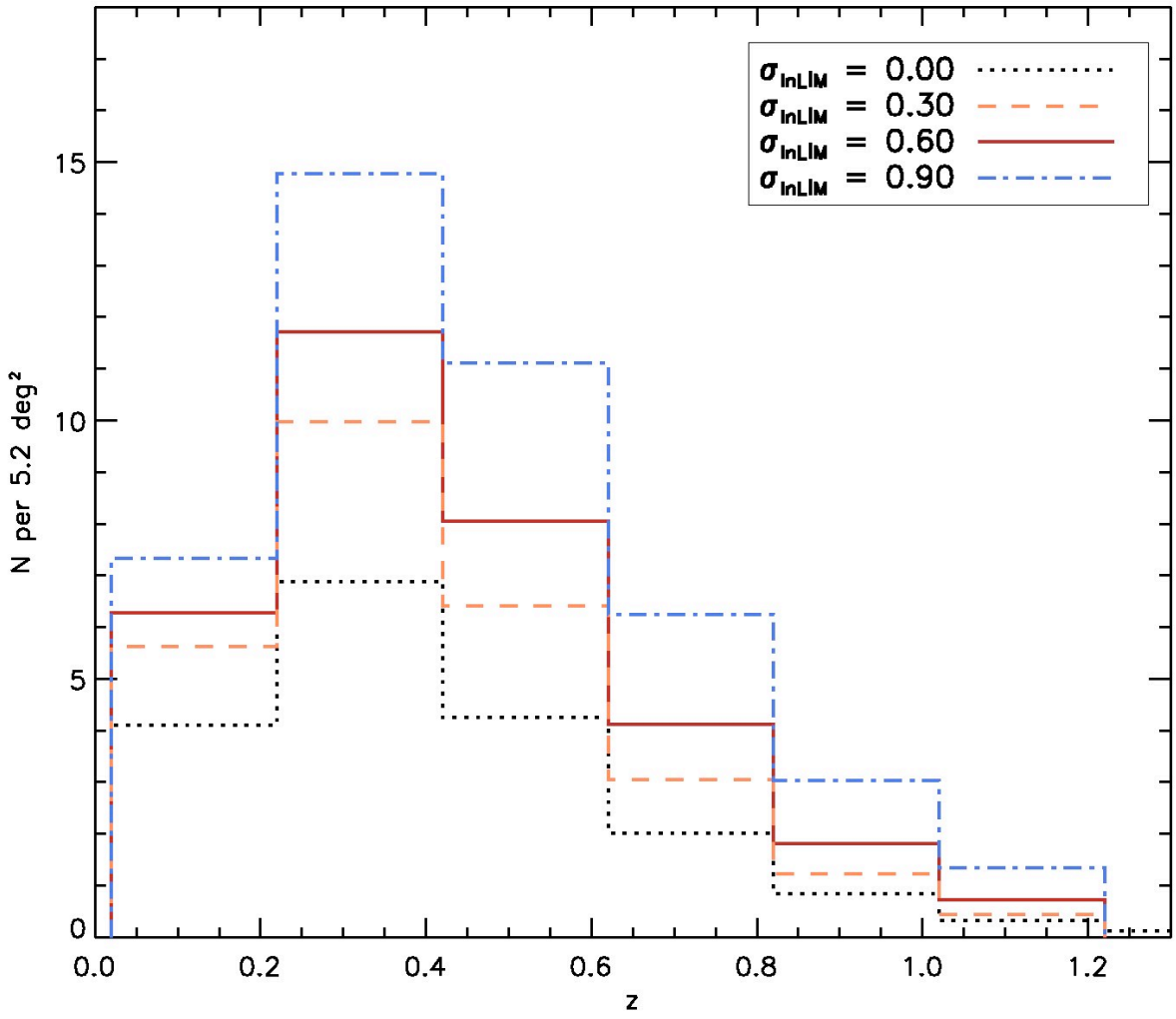

Fig. 3. Impact of the scatter in the M–Lx relation on the predicted C1 redshift distribution.
For simplicity, all the dispersion contained in the scaling laws is encapsulated in the M-L relation. For the above scatter values, the predicted total number of clusters per square degree are: 3.6 (no scatter), 5.1 (0.3) and 8.4 (0.9). The mean scatter value of 0.6 (adopted in PA07) corresponds to a number density of 6.2/deg^2.

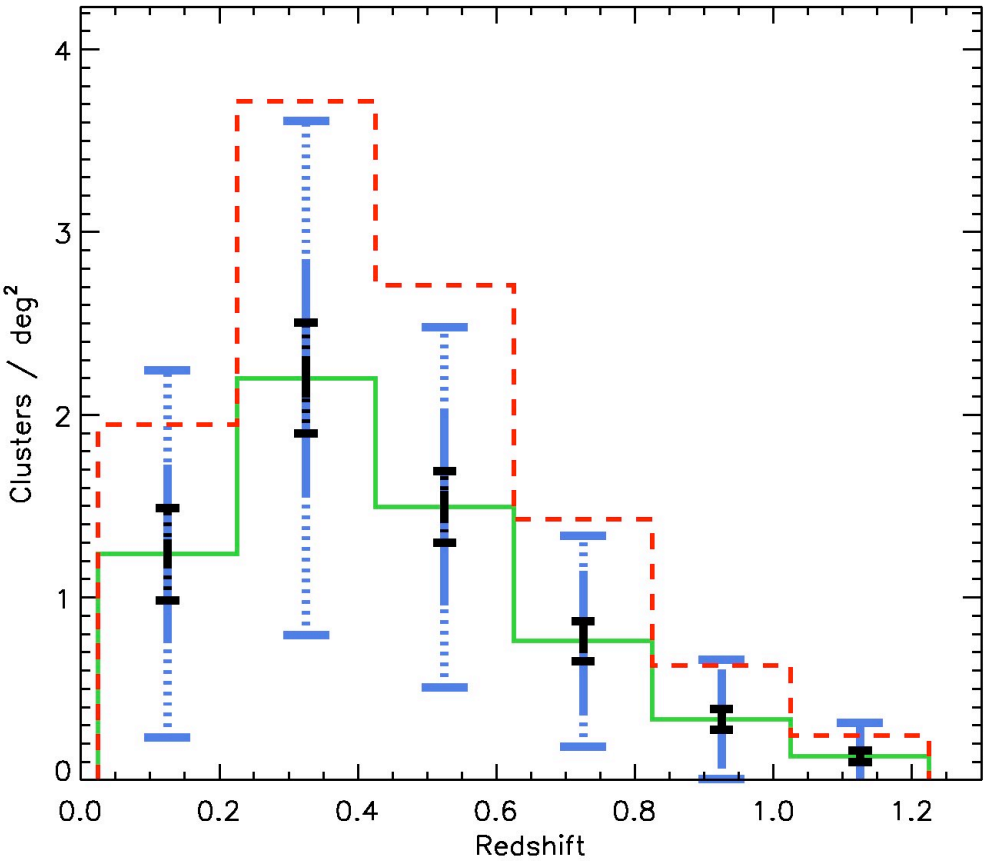

Fig. 4 Predicted dn/dz distribution for the C1 cluster population over 200 deg^2.
The solid green histogram shows the expectations of our cosmological model (WMAP3: σ8 = 0.74 and self- similar evolution for the Lx-T relation). Fluctuations around the mean expectation are represented by the solid and dotted error bars for respectively the shot noise alone and shot noise + sample variance (estimated from Hu & Kravtsov 2003). The blue error bars are for 5 deg^2 (published XMM-LSS sample), while the black ones stand for 200 deg^2. For comparison, the dashed-line red histogram shows the predictions for a model with WMAP 1st year cosmological parameters (σ 8 = 0.85) where the expected cluster density has been lowered by assuming a non-evolving Lx-T relation.

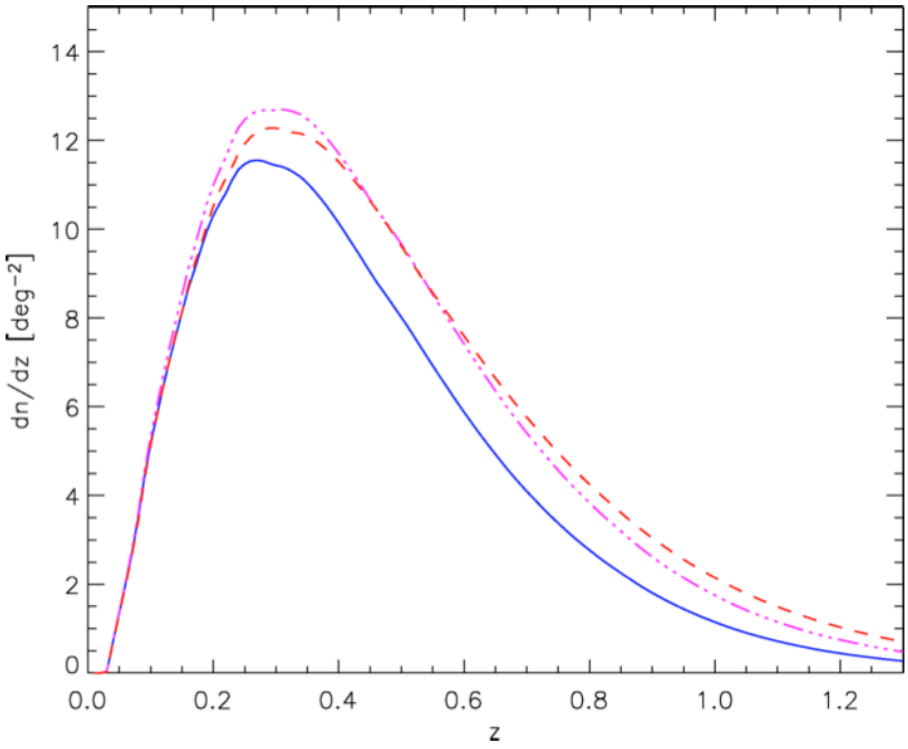

Figure 5. Impact of the cluster scaling laws in the determination of the Dark Energy equation of state (from our model – thus, assuming an infinite number of clusters)

The solid line shows the prediction for the Spergel et al. (2007) cosmology and self-similar evolution of the scaling laws. Assuming instead $F(z) = E(z) \times (1 + z)^{0.34}$ for the L–T evolution, which is the 1σ higher bound from the current XMM-LSS data, yields the dot–dashed line. As a comparison, the dashed line shows the distribution obtained by keeping self-similar evolution but changing the dark energy equation of state from –1 to –0.6.

References:

Pacaud, F. et al: 2007, MNRAS 382, 1289 (PA07)
Spergel, D. N. et al: 2003, ApJS,148, 175
Spergel, D. N. et al: 2007, ApJS 170, 377
Willis, J. P. et al.: 2005, MNRAS 363, 675